Inorganic Chemistry

ARTICLE

pubs.acs.org/IC

Single-Crystal Bi_2S_3 Nanosheets Growing via Attachment−Recrystallization of Nanorods

Hua Zhang, Jing Huang, Xinggui Zhou, and Xinhua Zhong*

State Key Laboratory of Chemical Engineering, Department of Chemistry, East China University of Science and Technology, Shanghai 200237, China

Supporting Information

ABSTRACT: High-quality Bi_2S_3 discrete single-crystal nanosheets with orthorhombic structure have been synthesized through the thermal decomposition of a single-source precursor, $Bi(S_2CNEt_2)_3$, in amine media. The morphology evolution reveals that the Bi_2S_3 nanosheets are developed through the assembly of nanorods, and an attachment−recrystallization growth mechanism is proposed for the formation of nanosheets with the use of nanorods as building blocks. High-resolution transmission electron microscopy studies reveal that the nanosheets have the largest exposed surface of (100) facets. The effects of experimental variables, such as the reaction temperature, time, precursor concentration, and media, on the morphology of the obtained nanocrystals have been systematically investigated in which the amine has served as the solvent, surfactant, and electron donor.

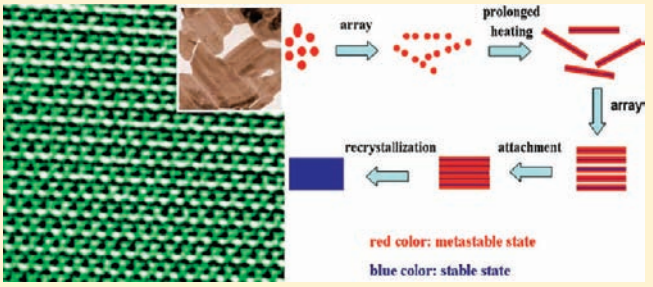

INTRODUCTION

Nanomaterials with different shapes such as nanodots, nanorods, and nanosheets have been widely studied on their synthesis, structure, and properties.[1] Recent flourishing studies on the structure, property, and application of graphene demonstrate the more importance of two-dimensional (2D) materials for their potential utilization.[2] Metal chalcogenides and oxides in the form of nanosheets have also attracted extra interest in their fabrication and characterization.[3] One characteristic of 2D single-crystal nanosheets is that they always have a large percentage of a specific crystal facet exposed. The study of Ohno et al. demonstrated that different surface energy levels of the conduction and valence bands are expected for different crystal facets of semiconductors because of the atomic arrangements characteristic of these facets.[4] The difference in the energy levels drives the electrons and holes to different crystal facets, leading to the separation of electrons and holes, which is very important for enhancement of the photocatalytic activity and photoelectric conversion. For example, TiO_2 nanosheets with exposed high reactive {001} facets played an important role in the high photocatalytic activity and improved photoelectric conversion efficiency.[5]

Bismuth sulfide (Bi_2S_3), a typical lamella-structured semiconductor with a bulk direct band gap of 1.3 eV,[6] has attracted much attention because of its potential applications such as in electrochemical hydrogen storage, X-ray-computed tomography imaging, biomolecule detection, photocatalyst, photoresponse, etc.[7] A series of Bi_2S_3 nanomaterials have been prepared via different methods including the solvothermal method, chemical vapor deposition, and a hot injection technique.[8] Previous reports have mainly focused on zero-dimensional (0D) Bi_2S_3 nanodots and one-dimensional (1D) nanorods and nanowires. Although the intrinsic highly anisotropic structure with a chain parallel to the *c* axis is favorable for the growth of 1D Bi_2S_3 nanostructures,[9] the lamellar structure similar to that of graphene and graphene oxide is also possibly the intrinsic driving force for the growth of 2D nanostructures. Several three-dimensional (3D) structures composed of 2D sheets have also been fabricated.[10] For example, Bi_2S_3 matlike polycrystallized architectures composed of perpendicularly assembled nanorods have been reported by the Li group via a seed-assistant hydrothermal route.[10c] Flower-like microstructures assembled by several sheets have been prepared by the Wang group.[10e] Chrysanthemum-like Bi_2S_3 microcrystals made of sheets have been reported by Liu and co-workers.[10a] Most of these high-dimensional structures are constituted of 1D or 2D building blocks connecting at a common part. To the best of our knowledge, no discrete 2D single-crystal Bi_2S_3 nanosheets have been reported, and it is still a great challenge to synthesize Bi_2S_3 nanosheets.

For most of nanosheets, including graphene, graphene oxide, and metal sulfides and oxides, the growth mechanism could be explained by cleavage or breakage,[11] epitaxial growth,[12] continuous lateral extension,[13] lamella-like templating,[14] exfoliation,[15] unzipping of the nanotubes,[16] oriented 2D attachment−self-organization followed by recrystallization,[17] and the assembly of thin superstructures.[18] For example, among bottom-up methods, continuous lateral extension of small spherical CdSe particles has been observed during the formation of CdSe nanoplates.[13] Cubic

Received: April 20, 2011
Published: July 20, 2011

PbS nanosheets[17a] and ceria nanosheets[17b] have been fabricated through the mechanism of 2D oriented attachment or self-organization of the initially formed small nanoparticles followed by an in situ recrystallization. In these cases, small particles with diameters of less than ~2 nm served as building blocks, or the growth of 2D plates started with ~2 nm particles. How to prepare single-crystal individual Bi_2S_3 nanosheets as well as determining the growth mechanism encourages us to investigate the preparation, structure, and growth mechanism of 2D Bi_2S_3 nanostructures.

Herein, high-quality orthorhmbic structured Bi_2S_3 single-crystal nanosheets are controllably prepared via a convenient single-source precursor approach by varying the experimental parameters including the precursor concentration, reaction temperature, time, and solvent in which $Bi(S_2CNEt_2)_3$ was used as the precursor. Electron microscopy studies demonstrate that the nanosheets evolve from nanorods and the possible growth mechanism of the sheets could be explained by attachment—recrystallization of the initially formed metastable nanorods.

EXPERIMENTAL SECTION

Chemicals. Sodium diethyldithiocarbamate trihydrate ($NaS_2CNEt_2 \cdot 3H_2O$) and bismuth chloride ($BiCl_3$, AR) were purchased from Sinopharm Chemical Reagent Co. Ltd. Oleylamine (OAM; 90%) was obtained from Acros and 1-dodecylamine (DDA) from Alfa Aesar. All of the chemicals were used as received without further purification. Double-distilled water was used throughout the experiments.

Preparation of the Precursor $Bi(S_2CNEt_2)_3$ and Stock Solution. A total of 33 mL of a 0.1 M $BiCl_3$ aqueous solution (containing some hydrochloric acid to prevent hydrolysis) was added dropwise to 100 mL of a 0.1 M NaS_2CNEt_2 aqueous solution under vigorous stirring. Yellowish precipitates formed immediately, and the reaction was stopped after about 30 min. The precipitates were collected via centrifugation, purified by washing several times with distilled water and methanol, and then dried in a vacuum at 60 °C for 5 h to obtain a $Bi(S_2CNEt_2)_3$ dry powder. For preparation of the stock solution, 65.4 mg of $Bi(S_2CNEt_2)_3$ powder was added to a flask containing 4.0 mL of OAM or DDA, followed by degassing at room temperature for 5 min under a vacuum to remove the moisture and oxygen. The reaction vessel was then filled with nitrogen, and the temperature was increased to 60 °C and kept at this temperature for 4 h to give a black heterogeneous solution, followed by natural cooling to room temperature.

Synthesis of Bi_2S_3 Nanosheets. A total of 20 mL of DDA in a three-necked flask was degassed at 60 °C, and the flask was filled with nitrogen, followed by an increase in the temperature to 220 °C. At this temperature, 2.0 mL of the stock solution prepared in DDA was injected into the flask and maintained for another 150 min. The growth of samples was terminated by removing the heating apparatus. The reaction mixture was cooled to room temperature, precipitated by anhydrous ethanol, and washed several times, and the purified nanocrystals were redispersed in hexane or toluene. The nanosheets could also be prepared in OAM but with low yield.

Characterization. The purity and crystalline structure of the products were confirmed by powder X-ray diffraction (XRD) obtained on a D8 Advance (Bruker) X-ray diffractometer equipped with graphite-monochromatized high-intensity Cu Kα radiation (λ = 0.154 06 nm) at 40 kV and 40 mA. Transmission electron microscopy (TEM) measurements were performed on a JEOL-1400 transmission electron microscope with an acceleration voltage of 100 kV. High-resolution TEM (HRTEM), electron diffraction (ED), and energy-dispersive spectrometry (EDS) were performed on a JEOL-2010 high-resolution electron microscope with an acceleration voltage of 200 kV. The samples were prepared by dropping a diluted solution of nanostructures in toluene on a carbon-coated copper grid and slowly drying in air.

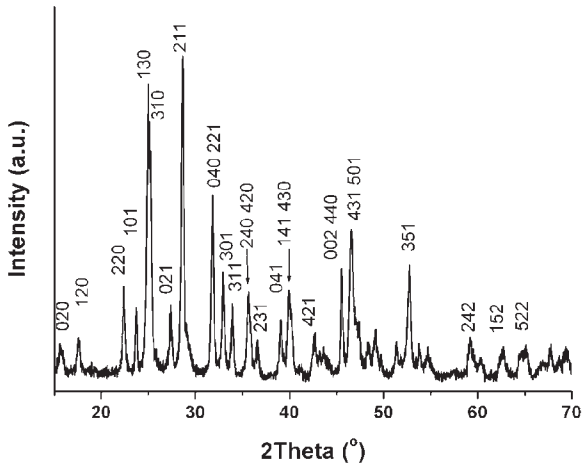

Figure 1. XRD pattern of Bi_2S_3 nanosheets.

RESULTS AND DISCUSSION

Preparation of the Precursor and Decomposition of the Stock Solution. In previous work,[9b,19] the precursor for preparing Bi_2S_3 nanostructures, dialkyldithiocarbamate complexes of bismuth(III), was often obtained from the reaction between bismuth oxide or bismuth nitrate and NaS_2CNEt_2 in methanol/acetone media with a reaction time up to 40 h. In some cases, CS_2 was used to react with amine to obtain sodium dialkyldithiocarbamate.[9b] Herein, we prepared the precursor $Bi(S_2CNEt_2)_3$ in aqueous media through the reaction between $BiCl_3$ and NaS_2CNEt_2. High yield (about 70%), short reaction time (about 0.5 h), no organic solvent, and a simple procedure are the prominent advantages of our approach. A mass spectrum (Figure S1 in the Supporting Information, SI) shows the existence of $[Bi(S_2CNEt_2)_2]^+$ consistent with literature data.[19e] Thermogravimetric analysis (TGA; Figure S2 in the SI; Perkin-Elmer TG/DTA 6300 thermoanalyzer, 10 °C/min heating rate, N_2 atmosphere) shows that the precursor in a dry powder form began to decompose slowly at ~165 °C, and the weight loss was only ~1.7% up to ~230 °C, starting from which the decomposition sped up, with the loss reaching to ~50% at 350 °C. When the precursor stock solution in OAM was maintained at 60 °C for 4 h, the initial clear solution turned turbid and precipitates could be obtained after centrifugation. To investigate evolution of the precursor in the stock solution, XRD and TEM were recorded as shown in the SI. In comparison with the XRD pattern of the precursor, there are no any new peaks observed in the stock solution, indicative of no new crystalline phase formed, while several diffractions disappeared (at about 18.3° and 39.5°) and some were enhanced (at about 24.0°, 36.4°, and 55°). This could be attributed to the little changes in the crystal structure, possibly resulting from the rearrangement of some atoms. When the stock solution was maintained at 180 °C for 2 min (with the XRD pattern shown in Figure S3 in the SI), a new peak centered at about 45.5° was distinctly observed and could be indexed to 130 facets of Bi_2S_3. Meanwhile, the remarkably enhanced peak at ~25.0 might come from 310 facets of Bi_2S_3 that overlapped with the precursor. The TEM images corresponding to the three

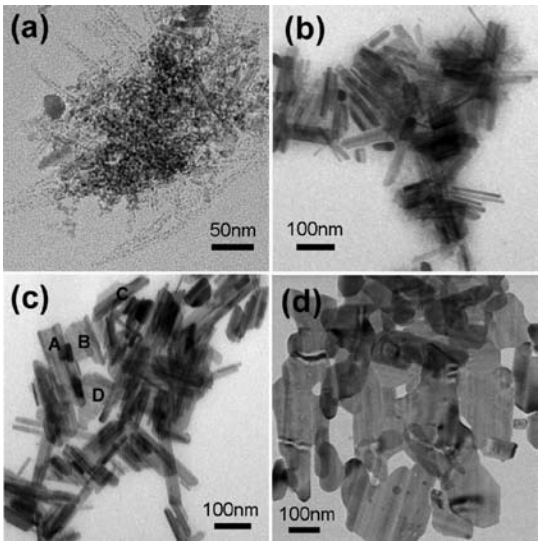

Figure 2. TEM images of Bi_2S_3 nanocrystals prepared at 220 °C for different reaction times of (a) 2, (b) 30, (c) 90, and (d) 150 min.

cases are shown in Figure S4 in the SI. The diameter change of the spherical particles from large to small (from ~6.0 to 4.8 nm and then to 3.5 nm) in combination with the XRD results exhibits decomposition of the precursors under different conditions, in which the high temperature was favorable for the growth of crystalline Bi_2S_3 particles.

Characterization of Bi_2S_3 Nanostructures. The phase structure of the as-prepared samples was characterized by XRD with the typical pattern shown in Figure 1. All of the diffraction peaks can be indexed to orthorhombic structured Bi_2S_3 with lattice constants of a = 11.14 Å, b = 11.30 Å, and c = 3.98 Å (JCPDS no. 17-0320), and the major peaks can be ascribed to the 020, 120, 220, and 130 facets. The phase purity is confirmed by the absence of other peaks.

Figure 2 shows the temporal evolution of TEM images of Bi_2S_3 nanostructures prepared at 220 °C in OAM media. With extension of the heating time, the nanostructure shapes evolved from dot to rod and finally to sheet. When the heating time was 2 min, the samples (Figure 2a) were dominantly composed of the spherical structures, commonly named nanodots, that have average diameters of about 4 nm, slightly larger than those prepared under 180 °C for 2 min (Figure S4c in the SI). It should be noted that some particles obviously have a tendency to assemble into lines. When the heating time was increased to 30 min, some rod-shaped nanorods were observed with diameters ranging from ~6 to 25 nm (Figure 2b). When the heating time was further increased to 90 min, nanorods and sheetlike morphologies coexisted in the sample (Figure 2c). It is interesting that the sheets are seemingly composed of several rods combining side-by-side. For example, in part A, the sheet is constituted of three rods with diameters of ~24 nm in uniform length, while rods in different lengths could assemble into irregular sheets like that in parts B–D. The difference in the widths of sheets comes from different amounts of rods. Figure 2d shows the typical TEM image of Bi_2S_3 nanosheets after 150 min of heating time, with the ED pattern and HRTEM images from a single sheet, as shown in Figure 3. (020) and (001) facets with continuous lattice fringes of about 0.560 and 0.398 nm consistent with the ED pattern, respectively, could be observed from the

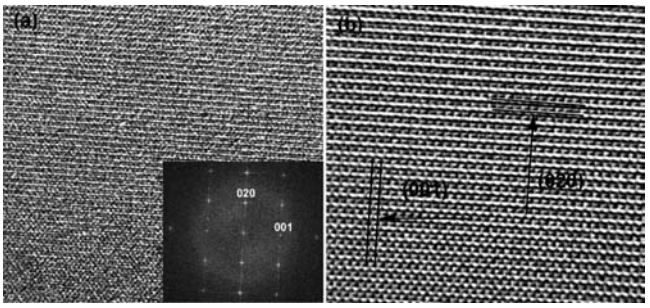

Figure 3. (a and b) HRTEM images of a high-quality single-crystal Bi_2S_3 nanosheet. Inset: corresponding Fourier transition pattern.

HRTEM image, indicating the high crystallinity and high quality of the obtained single-crystal nanosheets. From the ED and HRTEM results, it is reasonable to conclude that the nanosheets have the largest exposed surface of (100) facets other than (001) and (010) because of their perpendicularity to each other. In the previously observed matlike structure,[10c] Bi_2S_3 nanorods were the building blocks that aligned in two perpendicular directions. Therefore, the network in the form of sheets was polycrystalline, which was confirmed by ED patterns and TEM and scanning electron microscopy images. However, in our current work, the nanosheets exhibit the nature of high-quality single crystallinity that assembled nanorods through side-by-side contact only in one direction.

To further investigate the growth process of Bi_2S_3 single-crystal nanosheets, a series of samples were prepared under different experimental conditions. As shown in Figure 4a, when the stock solution was heated at 180 °C for 30 min, uniform nanorods with diameters of about 25 nm and lengths from 260 to 790 nm were obtained. It is interesting to find that some nanorods stand shoulder-to-shoulder and get close to each other. Upon careful inspection of the contrast of an individual nanorod (with the high-magnified image shown in the inset of Figure 4a), most of the nanorods have shallow borders along the axial direction and it seems as if the nanorod had a black line in the center. The difference in contrast within a nanorod is very common in the obtained rodlike samples. For further investigation, the ED and HRTEM images were studied from a single nanorod and are shown in Figure 4b–d. In the ED pattern recorded from the nanorod displaying a black line in the center marked with an arrow, several amorphous diffraction rings could be seen besides a complete set of diffraction patterns from a single crystal, indicating the coexistence of amorphous borders and a well-crystallized center in the nanorod, with its HRTEM image shown in Figure 4b. According to the contrast of the HRTEM image, the cross section of a nanorod could be divided into two areas: a well-crystallized center surrounded by amorphous borders. The squared area was further magnified and is shown in Figure 4d, in which the obvious cross-lattice fringes exhibit good crystallinity of the center part. Lattice fringes with a spacing of ~0.560, 0.374, and 0.398 nm could be indexed to (020), (101), and (001) facets, respectively, consistent with the EDS pattern. It should be noted that in the ED pattern the diffraction spots of (440) and (002) are very close, but only (002) is perpendicular to (020). The above analyses illustrate that the nanorods grow preferentially along the [001] direction. The EDS results (Figure S5 in the SI) show that no other elements except Bi and S could be seen from the whole nanorods.

dx.doi.org/10.1021/ic201332n |*Inorg. Chem.* 2011, 50, 7729–7734

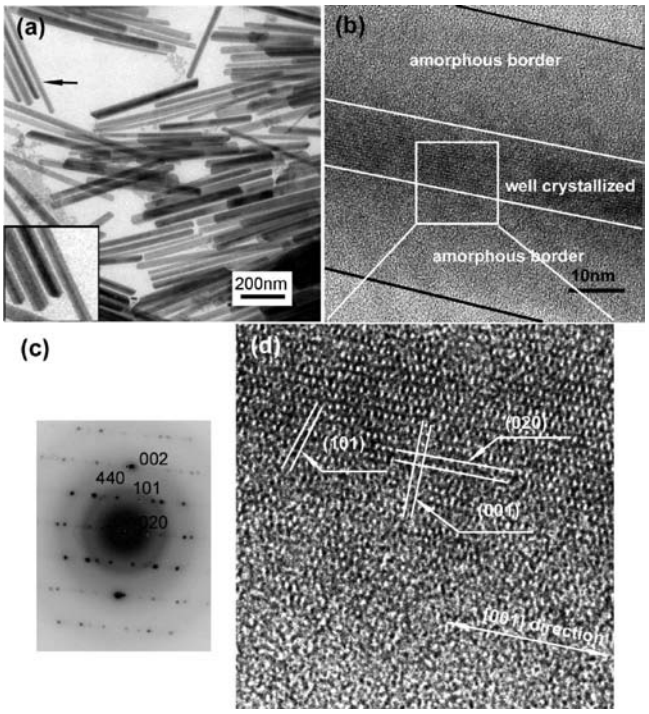

Figure 4. (a) Typical TEM image of nanorods in which the alignment and well-crystallized center are marked with an arrow and magnified in the inset. (b and d) HRTEM images of a single nanorod, with the corresponding ED pattern shown in part c displaying amorphous diffraction rings as well as a complete set of single-crystal diffraction patterns.

Influence of Experimental Variables on the Morphology of Nanostructures. It is found that high temperature and long reaction time are favorable for the formation of Bi_2S_3 nanosheets; however, dots and rods commonly coexisted in the sample, even though the reaction time was increased to 180 min. So, how to increase the efficiency of the assembly of rods and dots is the key factor for controlling the quality and yield of single-crystal nanosheets. A series of experiments were carried out at various conditions to optimize the variables for the preparation of Bi_2S_3 nanostructures with desired morphologies. The reaction time was severely restricted to 2 min during the synthesis of nanodots. The average diameters are ~3.5, 4.0, and 11.0 nm for samples prepared under 180, 220, and 260 °C (images not shown), respectively, demonstrating that higher temperature or longer time favors the larger size and high crystallinity. It has been established that a long reaction time would favor the large size and high yield of nanosheets, as demonstrated in Figure 2, where the morphologies of the obtained nanostructures evolved from dot to sheet with increasing reaction time. In order to prepare nanosheets with high quality and high yield, we further exploited the effect of the precursor concentration and nature of the reaction media. The lower concentrations termed as D2, D4, and D10 were realized by injecting the stock solution into reaction media that was preheated to a designed temperature with volumes of 2, 4, and 10 times as much as the injected one. From the experimental results shown in Figure 5, we find that a high reaction temperature, long reaction time, and low concentration favor high yields of well-crystallized, larger sized nanosheets. However, pure nanosheets could not be obtained under all of these conditions (i.e., nanodots and nanorods cannot be completely avoided). It is fortunate that when OAM was replaced with DDA, nanosheets with high quality and high yield could be successfully synthesized under 220 °C with 150 min of reaction time.

Growth Mechanism of Nanorods and Nanosheets. Under low temperature, the decomposition of precursor $Bi(S_2CNEt_2)_3$ in OAM media resulted in the formation of amorphous nanoparticles. It is well-known that amorphous particles have very high surface energy and are prone to congregate followed by recrystallization. When the unstable particles stand in line, 1D nanorods, or nanowires may finally form. The oriented attachment of small particles followed by the recrystallization process for nanorod or nanowire growth has been well studied in the literature.[20] From the experimental results, we think that the current growth of Bi_2S_3 nanorods could also be explained by this mechanism. The possible process is that the unstable nanodots assembled in a line, and with prolonged heating time, the attachment and recrystallization occurred, resulting in the formation of nanorods. However, the provided energy under a low temperature of 180 °C is deficient for complete crystallization and thus results in amorphous borders in nanorods. Meanwhile, according to ref 9a, the surface energy is (001) > (100) > (010) (the last two are slightly different); once the chemical bond between Bi^{3+} and S^{2-} formed along [001], it was stable and very hard to cleave. When the reaction temperature is further raised to 220 °C, which could provide additional energy, the nanorods possessing an unstable surface located at the border area could assemble and thermodynamically recrystallize, with the result being single-crystal nanosheet formation. Apparently, the Bi_2S_3 nanosheets have evolved from nanoparticles and nanorods. However, the typical proposed growth mechanisms like continuous lateral extension[13] and 2D self-organization[17a,b] are unsuitable to explain the current growth of Bi_2S_3 single-crystal nanosheets. On the basis of direct TEM observations, the attachment of the initially formed unstable nanorods as building blocks followed by a thermodynamic recrystallization process could reasonably explain the Bi_2S_3 nanosheet growth. The attachment−recrystallization growth mechanism for the fabrication of nanorods and nanosheets is simply clarified in Scheme 1. Few works have been reported on the preparation of high-dimensional nanostructures in which nanorods served as building blocks, but they are different from our side-by-side attachment. For example, the nanorods could self-assemble with a certain angle into twinned triangle-shaped feitknechtite particles.[21] CdS nanosheets have been prepared from side branching of secondary nanowires perpendicular to the original nanowires and filling between them.[22] The driving force for the spontaneous attachment and recrystallization of Bi_2S_3 particles is, from a thermodynamic viewpoint, the essential reduction in the surface energy.[17d]

Effective assembly of the initially formed dots and rods could be controlled by amine including OAM and DDA. The metal precursor and amine were only involved in the reaction, so the amine could reasonably serve as both of the reaction media and surfactant. The amine-capped Bi_2S_3 nanorods showed a remarkable tendency to organize, and the distance between the side-by-side nanorods is different from the length of an amine molecule.[23] The tendency to organize was also confirmed in our previous work.[7d] The structural differences between OAM and DDA lie in the length and carbon bond type, which are indicated in Scheme 2. In the preparation of the stock solution, it should be noted that it took only about 45 min for the precursor solution in DDA to turn black, indicating decomposition of $Bi(S_2CNEt_2)_3$,

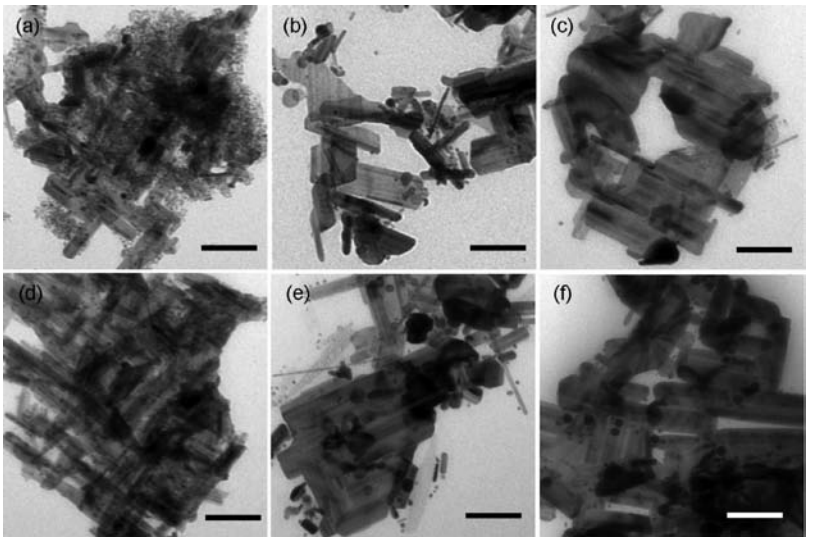

Figure 5. Effect of the reaction temperature, concentration, and time on the morphology of Bi_2S_3 nanocrystals with samples marked as temperature (°C)−diluted concentration−time (min): (a) 220−D5−5; (b) 220−D5−60; (c) 220−D5−90; (d) 180−D10−90; (e) 220−D10−90; (f) 260−D5−60. The scale bars are 200 nm.

Scheme 1. Attachment−Recrystallization Growth Mechanism of Nanorods and Single-Crystal Nanosheets Evolving from Amorphous Nanodots and Metastable Nanorods, Respectively

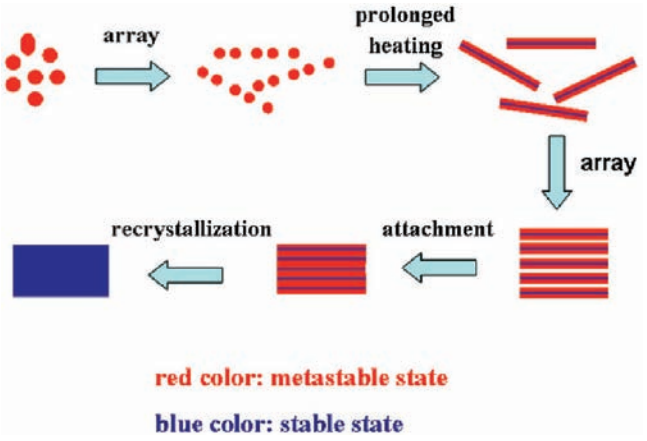

Scheme 2. Decomposition of the Precursor in an Amine Solvent

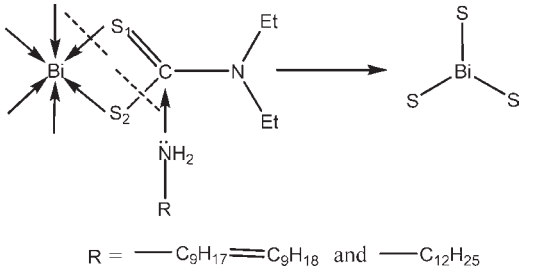

while that in OAM took about 90 min. It is safe to say that thermal decomposition of $Bi(S_2CNEt_2)_3$ is easier in DDA than in OAM media. In other words, we think that DDA is favorable for decomposition of $Bi(S_2CNEt_2)_3$ and could speed the nucleation of Bi_2S_3. The nanostructured Bi_2S_3 synthesized from bismuth dithiocarbamate was reported in a previous paper,[24] where free protons from water or another solvent approached between the nitrogen and sulfur atoms to form a hydrogen bond, which promoted the attack of a hydroxide anion on the electrophilic site of the ligand, i.e., the thiocarbamate carbon atom. In the meantime, rodlike Bi_2S_3 could only be obtained in a protic solvent. In our experiments, organic amine was used as the solvent and there was no existence of a free photon from water. The formation of metal sulfide is briefly illustrated in Scheme 2. Similar to a hydroxide anion, the electron donor, i.e., amido, attacked the thiocarbamate carbon atom, resulting in C−S bond cleavage, followed by cleavage of the S−Bi bond. Further cleavage and the formation of Bi_2S_3 were driven by precipitation. DDA is more favorable than OAM for cleavage and could promote the nucleation of Bi_2S_3, while in OAM, the existence of a C=C double bond possibly weakens the attack of amido. This also means that DDA is better at improving the growth of Bi_2S_3 nanosheets than OAM in the present experiments. The exact reason currently could not be further confirmed and is still worth studying in the next work.

CONCLUSION

In summary, a single-source precursor route has been demonstrated for the synthesis of shape-controllable Bi_2S_3 nanocrystals in the form of nanodots, nanorods, and nanosheets; especially the high-quality discrete single-crystal nanosheets with the largest exposed surface of (100) facets accompanied by perpendicular (001) and (010) are first fabricated in high yield and good crystallinity. On the basis of the direct TEM inspection, the attachment−recrystallization growth mechanism for nanosheets evolving from metastable nanorods as building blocks has also been proposed in which the driving force could be the reduction in the surface energy. The amine serves as the reaction media, surfactant, and electron donor in the formation of Bi_2S_3 nanocrystals,

dx.doi.org/10.1021/ic201332n |*Inorg. Chem.* 2011, 50, 7729–7734

and DDA could improve the quality and yield of the sheets rather than OAM. These findings further expand our expectation on the synthesis and potential application of single-crystal Bi_2S_3 nanosheets with the largest exposed active (001) facets.

■ ASSOCIATED CONTENT

Supporting Information. Mass spectrum, a TGA curve, and XRD patterns of the precursor, TEM images, and an EDS pattern. This material is available free of charge via the Internet at http://pubs.acs.org.

■ AUTHOR INFORMATION

Corresponding Author

*E-mail: zhongxh@ecust.edu.cn. Fax: +86 21 6425 0281.

■ ACKNOWLEDGMENT

We thank the National Natural Science Foundation of China (Grants 20771037 and 20871047), the Fundamental Research Funds for the Central Universities, the State Key Laboratory of Chemical Engineering (No. SKL-ChE-09C01), and the Program for Professor of Special Appointment at Shanghai Institutions of Higher Learning for financial support.

■ REFERENCES

(1) (a) Zhang, F.; Wen, M.; Cheng, M.; Wu, Q. S.; Meng, X. G. *J. Mater. Chem.* **2010**, *20*, 7661–7668. (b) Liu, X.; Guo, G. C.; Wu, A. Q.; Cai, L. Z.; Huang, J. S. *Inorg. Chem.* **2005**, *44*, 4282–4286. (c) Deng, B.; Zhong, S. L.; Wang, D. H.; Wang, S. S.; Zhang, T. K.; Qu, W. G.; Xu, A. W. *Nanoscale* **2011**, *3*, 1014–1021. (d) Webber, D. H.; Brutchey, R. L. *Inorg. Chem.* **2011**, *50*, 723–725.

(2) (a) Ruben, M. B.; Cristing, G. N.; Julio, G. H.; Felix, Z. *Nanoscale* **2011**, *3*, 20–30. (b) Allen, M. J.; Tung, V. C.; Kaner, R. B. *Chem. Rev.* **2010**, *110*, 132–145. (c) Brownson, D. A. C.; Kampouris, D. K.; Banks, C. E. *J. Power Sources* **2011**, *196*, 4873–4885.

(3) (a) Dong, G. H.; Zhu, Y. J.; Chen, L. D. *J. Mater. Chem.* **2010**, *20*, 1976–1981. (b) Umar, A.; Hahn, Y. B. *Nanotechnology* **2006**, *17*, 2174–2180. (c) Liu, J. H.; Wei, X. F.; Wang, X.; Liu, X. W. *Chem. Commun.* **2011**, *47*, 6135–6137. (d) Ma, R. Z.; Sasaki, T. *Adv. Mater.* **2010**, *22*, 5082–5104.

(4) (a) Ohno, T.; Sarukawa, K.; Matsumura, M. *New J. Chem.* **2002**, *26*, 1167–1170. (b) Murakami, N.; Kurihara, Y.; Tsubota, T.; Ohno, T. *J. Phys. Chem. C* **2009**, *113*, 3062–3069.

(5) (a) Wang, Z.; Lv, K.; Wang, G.; Deng, K.; Tang, D. *Appl. Catal., B* **2010**, *100*, 378–385. (b) Yu, J.; Fan, J.; Lv, K. *Nanoscale* **2010**, *2*, 2144–2149.

(6) Vogel, R.; Hoyer, P.; Weller, H. *J. Phys. Chem.* **1994**, *98*, 3183–3188.

(7) (a) Rabin, O.; Perez, J. M.; Grimm, J.; Wojtkiewicz, G.; Weissleder, R. *Nat. Mater.* **2006**, *5*, 118–112. (b) Li, L.; Sun, N.; Huang, Y.; Qin, Y.; Zhao, N.; Gao, J.; Li, M.; Zhou, H.; Qi, L. *Adv. Funct. Mater.* **2008**, *18*, 1194–1201. (c) Bao, H.; Li, C. M.; Cui, X.; Song, Q.; Yang, H.; Guo, J. *Nanotechnology* **2008**, *19*, 335302. (d) Wu, T.; Zhou, X. G.; Zhang, H.; Zhong, X. H. *Nano Res.* **2010**, *3*, 379–386.

(8) (a) Stavila, V.; Whitmire, K. H.; Rusakova, I. *Chem. Mater.* **2009**, *21*, 5456–5465. (b) Wang, D. S.; Hao, C.; Zheng, W.; Ma, X.; Chu, D.; Peng, Q.; Li, Y. D. *Nano Res.* **2009**, *2*, 130–134. (c) Fan, D.; Thomas, P. J.; O'Brien, P. *Chem. Phys. Lett.* **2008**, *465*, 110–114. (d) Wang, D. S.; Zheng, W.; Hao, C. H.; Peng, Q.; Yi, Y. D. *Chem.—Eur. J.* **2009**, *15*, 1870–1875. (e) Cademartiri, L.; Malakooti, R.; O'Brien, P. G.; Migliori, A.; Petrov, S.; Kherani, N. P.; Ozin, G. A. *Angew. Chem., Int. Ed.* **2008**, *47*, 3814–3817.

(9) (a) Wang, Y.; Chen, J.; Wang, P.; Chen, L.; Chen, Y. B.; Wu, L. M. *J. Phys. Chem. C* **2009**, *113*, 16009–16014. (b) Shen, X. P.; Yin, G.; Zhang, W. L.; Xu, Z. *Solid State Commun.* **2006**, *140*, 116–119.

(10) (a) Jiang, J.; Gao, G.; Yu, R.; Qiu, G.; Liu, X. *Solid State Sci.* **2011**, *13*, 356–360. (b) Zhu, G. Q.; Liu, P. *Cryst. Res. Technol.* **2009**, *44*, 713–720. (c) Tang, C. J.; Zhang, Y. X.; Dou, X. C.; Li, G. H. *J. Cryst. Growth* **2010**, *312*, 692–697. (d) Zhang, H.; Wang, L. *Mater. Lett.* **2007**, *61*, 1667–1670. (e) Song, C. X.; Wang, D. B.; Yang, T.; Hu, Z. S. *CrystEngComm* **2011**, *13*, 3087–3092.

(11) (a) Li, J. M. *Appl. Phys. A: Mater. Sci. Process.* **2010**, *99*, 229–235. (b) Dong, X.; Wang, L.; Zhou, J.; Deng, L.; Huo, J.; Zhang, C. *J. Phys. Chem. B* **2006**, *110*, 13045–13049.

(12) (a) Reina, A.; Jia, X. T.; Ho, J.; Nezich, D.; Son, H.; Bulovic, V.; Dresselhaus, M. S.; Kong, J. *Nano Lett.* **2009**, *9*, 30–35. (b) Parga, A. L. V.; de Calleja, F.; Borca, B.; Passeggi, J. M. C. G.; Hinarejos, J. J.; Guinea, F.; Miranda, R. *Phys. Rev. Lett.* **2008**, *100*, 056807.

(13) Ithurria, S.; Bousquet, G.; Dubertret, B. *J. Am. Chem. Soc.* **2011**, *133*, 3070–3077.

(14) (a) Son, J. S.; Wen, X. D.; Joo, J.; Chae, J.; Baek, S.; Park, K.; Kim, J. H.; An, K.; Yu, J. H.; Kwon, S. G.; Choi, S. H.; Wang, Z.; Kim, Y. W.; Kuk, Y.; Hoffmann, R.; Hyeon, T. *Angew. Chem., Int. Ed.* **2009**, *48*, 6861–6864. (b) Wen, P.; Itoh, H.; Tang, W.; Feng, Q. *Langmuir* **2007**, *23*, 11782–11790.

(15) (a) Zimney, E. J.; Stach, E. A.; Piner, R. D.; Nguyen, S. T.; Ruoff, R. S. *Nature* **2006**, *442*, 282–286. (b) Fukuda, K.; Nakai, I.; Ebina, Y.; Ma, R.; Sasaki, T. *Inorg. Chem.* **2007**, *46*, 4787–4791.

(16) (a) Kosynkin, D. V.; Higginbotham, A. L.; Sinitskii, A.; Lomeda, J. R.; Dimiev, A.; Price, B. K.; Tour, J. M. *Nature* **2009**, *458*, 872–U5. (b) Cano-Marquez, A. G.; Rodríguez-Macías, F. J.; Campos-Delgado, J.; Espinosa-Gonzalez, C. G.; Tristan-Lopez, F.; Ramírez-Gonzalez, D.; Cullen, D. A.; Smith, D. J.; Terrones, M.; Vega-Cantu, Y. I. *Nano Lett.* **2009**, *9*, 1527–1533. (c) Elías, A. L.; Botello-Mendez, A. R.; Meneses-Rodríguez, D.; Gonzalez, V. J.; Ramírez-Gonzalez, D.; Ci, L.; Munoz-Sandoval, E.; Ajayan, P. M.; Terrones, H.; Terrones, M. *Nano Lett.* **2010**, *10*, 366–372. (d) Jiao, L. Y.; Zhang, L.; Wan, X. R.; Diankov, G.; Dai, H. J. *Nature* **2009**, *458*, 877–880.

(17) (a) Schliehe, C.; Juarez, B. H.; Pelletier, M.; Jander, S.; Greshnykh, D.; Nagel, M.; Meyer, A.; Foerster, S.; Kornowski, A.; Klinke, C.; Weller, H. *Science* **2010**, *329*, 550–553. (b) Yu, T.; Lim, B.; Xia, Y. N. *Angew. Chem., Int. Ed.* **2010**, *49*, 4484–4487. (c) Xu, A. W.; Ma, Y.; Cölfen, H. *J. Mater. Chem.* **2007**, *17*, 415–449. (d) Xu, A. W.; Antonietti, M.; Cölfen, H.; Fang, Y. P. *Adv. Funct. Mater.* **2006**, *16*, 903–908.

(18) (a) Yang, H. G.; Zeng, H. C. *Angew. Chem., Int. Ed.* **2004**, *43*, 5930–5933. (b) Tang, Z. Y.; Zhang, Z.; Wang, Y.; Glotzer, S. C.; Kotov, N. A. *Science* **2006**, *314*, 274–278.

(19) (a) Albuquerque, R.; Neves, M. C.; Mendonca, M. H.; Trindade, T.; Monteriro, O. C. *Colloids Surf., A* **2008**, *328*, 107–113. (b) Raston, C. L.; White, A. H. *J. Chem. Soc., Dalton Trans.* **1976**, 791–794. (c) Monteiro, O. C.; Nogueira, H. I. S.; Trindade, T.; Motevalli, M. *Chem. Mater.* **2001**, *13*, 2103–2111. (d) Tahir, A. A.; Ehsan, M. A.; Mazhar, M.; Upul Wijayantha, K. G.; Zeller, M.; Hunter, A. D. *Chem. Mater.* **2010**, *22*, 5084–5092. (e) Li, H.; Lai, C. S.; Wu, J.; Ho, P. C.; Vos, D.; Tiekink, E. R. T. *J. Inorg. Biochem.* **2007**, *101*, 809–816.

(20) (a) O'Sullivan, C.; Gunning, R. D.; Sanyal, A.; Barrett, C. A.; Geaney, H.; Laffir, F. R.; Ahmed, S.; Ryan, K. M. *J. Am. Chem. Soc.* **2009**, *131*, 12250–12257. (b) He, X.; Gao, L.; Yang, S.; Sun, J. *CrystEngComm* **2010**, *12*, 3413–3418. (c) Chen, M.; Xie, Y.; Lu, J.; Xiong, Y.; Zhang, S. Y.; Qian, Y. T.; Liu, X. M. *J. Mater. Chem.* **2002**, *12*, 748–753. (d) Zhang, J.; Huang, F.; Lin, Z. *Nanoscale* **2010**, *2*, 18–34.

(21) Portehault, D.; Cassaignon, S.; Baudrin, E.; Jolivet, J. P. *Cryst. Growth Des.* **2010**, *10*, 2168–2173.

(22) Choi, Y. J.; Choi, K. J.; Kim, D. W.; Park, J. G. *J. Nanosci. Nanotechnol.* **2009**, *9*, 4487–4497.

(23) Malakootim, R.; Cademartiri, L.; Akcakir, Y.; Petrov, S.; Migliori, A.; Ozin, G. A. *Adv. Mater.* **2006**, *18*, 2189–2194.

(24) Xie, G.; Qiao, Z. P.; Zeng, M. H.; Chen, X. M.; Gao, S. L. *Cryst. Growth Des.* **2004**, *4*, 513–516.